Fibers and Polymers 2021, Vol.22, No.1, 49-58
DOI 10.1007/s12221-021-0178-8

ISSN 1229-9197 (print version)
ISSN 1875-0052 (electronic version)

Electrically Conductive Nanofibers Composed of Chitosan-*grafted* Polythiophene and Poly(ε-caprolactone) as Tissue Engineering Scaffold

Bakhshali Massoumi[1], Mojtaba Abbasian[1], Balal Khalilzadeh[2,3], Rana Jahanban-Esfahlan[4,5], Hadi Samadian[6], Hossein Derakhshankhah[7], and Mehdi Jaymand[6]*

[1]*Department of Chemistry, Payame Noor University, Tehran, Iran*
[2]*Stem Cell Research Center, Tabriz University of Medical Sciences, Tabriz, Iran*
[3]*Biosensors and Bioelectronics Research Center, Ardabil University of Medical Sciences, Ardabil, Iran*
[4]*Department of Medical Biotechnology, Faculty of Advanced Medical Sciences, Tabriz University of Medical Sciences, Tabriz, Iran*
[5]*Student Research Committee, Tabriz University of Medical Sciences, Tabriz, Iran*
[6]*Nano Drug Delivery Research Center, Health Technology Institute, Kermanshah University of Medical Sciences, Kermanshah, Iran*
[7]*Pharmaceutical Sciences Research Center, Health Institute, Kermanshah University of Medical Sciences, Kermanshah, Iran*

(Received February 22, 2020; Revised April 2, 2020; Accepted April 8, 2020)

Abstract: Two novel electrically conductive nanofibrous scaffolds based on chitosan-*grafted* polythiophene (CS-*g*-PTh), and chitosan-*grafted* polythiophene/poly(ε-caprolactone) (CS-*g*-PTh/PCL) have been fabricated through electrospinning technique, and their performances in tissue engineering (TE) application were preliminary investigated in terms of biological (biocompatibility, biodegradability, and enhancing the cells adhesion and proliferation) as well as physicochemical (composition, electroactivity, conductivity, hydrophilicity, and morphology) features. The conductivities of the CS-*g*-PTh and CS-*g*-PTh/PCL nanofibrous scaffolds were determined as 0.09 and 8×10^{-3} Scm^{-1}, respectively. The developed CS-*g*-PTh/PCL scaffold exhibited slightly higher cells proliferation (8.24±0.49) than those of the CS-*g*-PTh scaffold (7.1±0.38) in time period of 7 days. The biodegradability tests using gravimetric approach revealed that the mass loss of CS-*g*-PTh and CS-*g*-PTh/PCL electrospun nanofibers were about 28.1 and 37.3 wt.%, respectively, at the end of experiments (sixth weeks). It was found that the electrospinning of CS-*g*-PTh with PCL improves the nanofibers uniformity as well as the biological features (*e.g.*, biocompatibility and cell proliferation) of the resultant scaffold.

Keywords: Chitosan, Polythiophene, Poly(ε-caprolactone), Nanofibers, Tissue engineering

Introduction

Tissue engineering (TE) is a multi-disciplinary science that introduced as a powerful approach for repair or regeneration of failed tissues/organs. This relatively new science is the base of living cells, signal molecules, and scaffolds [1-3]. Among these, the scaffold provides temporary three dimensional (3D) frameworks for seeded cells, and has essential role in their adherence, proliferation, and differentiation. An ideal scaffold shuold mimic the biomechanical function, as well as microstructural and topological characteristics of the native extracellular matrix (ECM) [4,5]. Therefore, a scaffold should meet some requirements, including high degree of porosity, high surface-to-volume ratio, appropriate pore size, and geometry control. Furthermore, other features of a suitable scaffold are proper cell-matrix interactions, excellent mechanical properties, appropriate chemical composition, biocompatibility, acceptable biodegradation and catabolization rates, as well as a simple and cost-effective fabrication technology [6,7]. In this context, electrospinning has been introduced as an efficient and powerful approach for the fabrication of nanofibrous porous scaffolds [8,9].

Numerous biomaterials, including synthetic or natural biomaterials, a combination of them, as well as natural acellular tissues have been applied as scaffolding. The most important issue regarding natural acellular scaffolds is their sources limitation. Therefore, synthetic or natural biomaterials are the most important options in the field [1,10]. In this context, polymeric biomaterials are particular of interest due to their superior characteristics, including excellent processability, biodegradability and biocompatibility, as well as tunable physicochemical and biological features [11,12]. Both synthetic and natural polymers have been employed as scaffolding material. However, natural polymers have been received more attention due to their some inherent properties over synthetic polymers that discussed in the following.

Natural polymers are categorized into three main classes, including polypeptides, polysaccharides, and polyesters [13,14]. The intense interest toward the fabrication of scaffolds based on natural polymers is arises from their superior features such as their extraordinarily elevated stability (in most cases), variable/controllable solubility, 3D geometry, low immunogenicity, excellent biocompatibility

*Corresponding author: m_jaymand@yahoo.com

and cytocompatibility, antigenicity, proper ECM mimicking, and good biodegradability [15,16]. However, several drawbacks of natural polymers, including batch to batch variation mainly due to their complex structure, morphology and chemical composition, high production cost in some cases (*e.g.*, hyaluronic acid and collagen), rapid degradation kinetics in some cases (*e.g.*, gelatin), uncontrolled rate of hydration, and possibility of microbial spoilage which may restrict their applications as scaffolding biomaterials [17,18]. In addition, some natural polymers suffer from poor processability (*e.g.*, cellulose and chitosan), and low mechanical properties (*e.g.*, polypeptides) [19,20]. To address these issues, the manipulation of these polymers is necessary for a successful TE purpose. For this purpose, the most exploited approaches are preparation of polymeric blends and composites using synthetic or semi-synthetic polymers [21], chemical [13] or physical [22] modifications, and physical or chemical [23] crosslinking strategies.

On the other hand, many research efforts have been devoted for development of electrically conductive scaffolds due to effect of electric fields or stimuli on the regaining of function in some damaged tissues/organs (*e.g.*, spinal cord), help to healing of chronic wounds and nerve regeneration, and enhance endochondral ossification [24-26]. These important advantages using electrically conductive scaffolds originates form their two important effects as follows:

1) Enhancing the signaling between the cells

2) Allows the local delivery of external electrical stimuli to the damaged site in order to enhance the healing procedure [27].

In this context, electrically conductive polymers (ECPs) can be considered as interested materials for scaffolding due to their exclusive features, including excellent electrical conductivity and compatibility with many cells/tissues in purified forms both *in vitro* and *in vivo* [28-30]. Among the ECPs, polythiophene (PTh) is particular of interest mainly due to its superior physicochemical properties, including excellent environmental stability, high and long term electrical conductivity, acceptable mechanical strengths, ease synthesis and low costs, as well as good *in vitro* and *in vivo* biocompatibility in purified form [31,32]. In addition, in TE based on electrically conductive scaffold cellular activities such as cell adhesion, migration, proliferation and differentiation, can be adjusted with or without external electrical stimulation [33]. Some research projects have been conducted for the fabrication of electroactive scaffolds for various types of TE. In a successful attempt, Wu and co-workers developed a highly tunable conductive biodegradable flexible polyurethane by polycondensation of poly(glycerol sebacate) and aniline pentamer to significantly enhance Myelination of Schwann cells (SCs) myelin gene expression and neurotrophin secretion for peripheral nerve TE. The results revealed that the developed scaffold has great potential for nerve regeneration applications [34]. In another study, Bagheri *et al*. fabricated electrically conductive nanofibers composed of chitosan-aniline oligomer/poly(vinyl alcohol) for TE purposes. The conductivity of the nanofibers was determined as 10^{-5} Scm^{-1}. The mechanical tests revealed that the oligoaniline addition enhanced the strength modulus and decreased the elongation at the break of nanofibers, mainly due to the rigid nature of the aniline oligomers. They concluded that the developed scaffold can be used for TE; as well as can be used as an on-demand stimuli-responsive dexamethasone release platform [35].

According to the above-mentioned facts, the association of natural and electrically conductive polymers can be considered as an efficient strategy to produce composite biomaterials for scaffolding with enhanced physicochemical as well as biological features. So, in continuation of our attention for developing electrically conductive biomaterials as TE scaffold [36-39], the aim of this study was to develop two novel electrically conductive nanofibrous scaffolds. For this purpose, chitosan was grafted with thiophene monomer through a chemical oxidation polymerization approach to produce a CS-*g*-PTh copolymer. The solution of CS-*g*-PTh copolymer with or without PCL solution were electrospun to afford conductive nanofibrous scaffolds. The biocompatibilities of the fabricated scaffolds were confirmed through assessing the adhesion, viability and proliferation of human liver cells (HEP G2).

Experimental

Materials

Thiophene monomer was purchased from Merck (Darmstadt, Germany), and was distilled twice under reduced pressure before use. Chitosan (medium molecular weight, extent of deacetylation 75-85 %), poly(ε-caprolactone) (M_n=70000-90000 $gmol^{-1}$), acetic acid, thiophene-2-carbaldehyde, sodium borohydride ($NaBH_4$), hydrogen peroxide (H_2O_2; 30 wt.%), anhydrous ferric chloride ($FeCl_3$), and tetraethylammonium tetrafluoroborate (TEAFB) were purchased from Sigma-Aldrich (St. Louis, MO, USA) and were used as received. All other chemical reagents were purchased from Merck or Sigma-Aldrich and purified according to the standard methods. Fetal bovine serum (FBS), MTT (3-(4,5-dimethylthiazol-2-yl)-2,5-diphe-nyltetrazolium bromide), phosphate buffered saline (PBS), and other biological reagents were purchased from Invitrogen (Carlsbad, CA, USA) and were used as received.

Synthesis of Thiophene-functionalized Chitosan Macromonomer (ThCSM)

In a 100-m*l* round-bottom flask equipped with a condenser, CS (2.00 g) was dissolved in an acetic acid solution (80 m*l*; 1 % v/v). After complete solubilization, thiophene-2-carbaldehyde (2.5 m*l*, 27 mmol) was added to the flask, and stirred for about 24 hours at room temperature. At the end of time, the reaction mixture was added dropwise into cold

methanol, filtered, washed several times with methanol, and the product obtained was dried in reduced pressure at room temperature.

The formed imine groups were reduced to more stable amine groups using $NaBH_4$ as follows. For this purpose, the synthesized product (2.00 g) was immersed in an aqueous acetic acid solution (80 m*l*; 1 % v/v) and stirred for about 3 hours. Afterwards, $NaBH_4$ (1.00 m*l*, 27 mmol) was added dropwise to the reactor. The content of the flask was stirred for about 12 hours at ambient condition. At the end of this time, the product was added dropwise into cold methanol, filtered, washed several times with methanol, and the product obtained was dried in reduced pressure at room temperature.

Synthesis of CS-*g*-PTh

A 250-m*l* three-necked round-bottom flask equipped with a condenser, dropping funnel, gas inlet/outlet, and a magnetic stirrer, was charged with ThCSM (1.50 g), and acetic acid solution (100 m*l* 1 % v/v). The mixture was refluxed at 60±3 °C for about 3 hours in order to complete solubilization the macromonomer. At the end of this time, the flask was cooled to room temperature, added thiophene monomer (2.00 m*l*, 25.5 mmol), and then the content of the flask was deaerated through the bubbling of argon gas for about 10 minutes.

In a separate container 6.20 g (38 mmol) of anhydrous ferric chloride was dissolved in 30 m*l* of distilled water. The oxidant solution was deaerated by bubbling argon gas for 10 minutes, and then added slowly to the above-mentioned flask under an argon protection. A small amount of hydrogen peroxide (2.00 m*l*, 30 wt.%.) was added to the flask in order to enhance the rate and yield of the reaction. The reaction mixture was refluxed for about 24 hours at room temperature. At the end of this time, the content of the flask was poured into a large amount of methanol in order to stop the polymerization. The product was filtered, and washed several times with methanol. The final black solid was dried in reduced pressure at room temperature.

Fabrication of CS-*g*-PTh and CS-*g*-PTh/PCL Nanofibers

The CS-*g*-PTh and CS-*g*-PTh/PCL nanofibers were fabricated through electrospinning technique as described in our previous works [9,39]. For the fabrication of CS-*g*-PTh nanofibers the sample was dissolved in dimethylsulfoxide; (DMSO; 3 % w/v), and then injected to the electrospinning equipment. However, in the case of CS-*g*-PTh/PCL nanofibers, the same volume solutions of the synthesized CS-*g*-PTh in DMSO (3 % w/v), and PCL in chloroform (1 % w/v) was injected to the electrospinning equipment.

Biocompatibility Experiments

Cell Culture

The human HEP G2 cells were cultured in complete Roswell Park Memorial Institute medium (RPMI-1640, Gibco, Invitrogen, Paisley, UK) supplemented with FBS (10 % v/v), and antibiotics (100 U cm^{-3} penicillin G, 0.1 mg cm^{-3} streptomycin, Invitrogen, CA, USA). The cells were incubated in a humidified incubator with CO_2 (5 %) at 37 °C in a water saturated atmosphere [40].

Cell Viability Assay

The cytotoxicity of the fabricated CS-*g*-PTh and CS-*g*-PTh/PCL nanofibers were evaluated against human HEP G2 cells through MTT colorimetric assay. In brief, 96-well plates were coated with sterilized (using gamma radiation) electrospun nanofibers, then the cells (15×10^3 cells per well) were seeded and allowed to attach overnight. Afterward, the plates incubated for about 48 hours, and then the media was replaced with a fresh media containing MTT (50 m*l*, 2 mgm^{-1} in PBS), and the cells were incubated for another 4 hours. Then, the formed formazan crystals were dissolved through the replacement of growth medium with DMSO (200 μ*l*) containing Sorensen's buffer (25 μ*l*; 0.133 M, pH 7.2). The quantity of produced purple color was measured at 570 nm using spectrophotometric microplate reader. It is worth to note that all experiments were carried out in triplicate [40].

Cell Growth Assay

The adhesion and proliferation of human HEP G2 cells onto the fabricated nanofibers were quantified using direct counting by hemocytometer. Briefly, the 16-well plates were coated with pre-sterilized CS-*g*-PTh and CS-*g*-PTh/PCL nanofibers, and then the cells were seeded at seeding density of 10^5 cells per well. The RPMI-1640 was added to each well, and the wells were maintained for 7 days at 37 °C under 5 % CO_2 atmosphere with medium refreshing every two days. The cells were detached through tripsinization, and further trypsin was deactivated using more media. Finally, cell sample was mixed with trypan blue (1:1 v/v), and the clear blue viable cells were count using hemocytometer slide.

Cell Morphology Study

The morphologies of the attached cells onto the fabricated nanofibers were observed using field emission-scanning electron microscope (FE-SEM). For this purpose, six-well plates were pre-coated with pre-sterilized nanofibers, and then the human HEP G2 cells were seeded at a seeding density of 5×10^4 cells per well. After incubation for about 24 hours in a humidified incubator, the cells were washed with double distilled water (DDW), and fixed with glutaraldehyde (2 wt.%, Sigma-Aldrich, USA) for about 1 hour at room temperature. The cells were washed with DDW several times, and dried at room temperature.

Characterization

Fourier transform infrared (FTIR) spectra were recorded using a Shimadzu 8101M FTIR (Kyoto, Japan) at room temperature. The samples were prepared in the pellet form

with potassium bromide (KBr) powder. The spectra were measured at a wavenumber resolution of 4 cm^{-1} as single scan for a spectral range from 400 to 4000 cm^{-1}. Proton nuclear magnetic resonance (^1H NMR) spectroscopy was performed on an FT-NMR Bruker spectrometer (Bruker, Ettlingen, Germany) with an operating frequency of 400 MHz at 25 °C. The field emission-scanning electron microscope (FE-SEM) type 1430 VP (LEO Electron Microscopy Ltd., Cambridge, UK) was applied to determine the morphologies of the synthesized samples as well as cells morphologies at operating voltage of 15 kV. Electrochemical experiments were carryout using an Auto-Lab PGSTA T302N electrochemical analysis system and GPES 4.7 software package (ECO chemie, the Netherlands). The conductivities of the samples were determined using the standard four-probe technique (Azar Electrode, Urmia, Iran) at ambient condition. The wettability of the samples were examined by water drop contact angle measurement using an OCA 20 plus contact angle meter system (Data physics Instruments GmbH, Filderstadt, Germany). The droplet size was 50 μ*l*, and all experiments were done in triplicates.

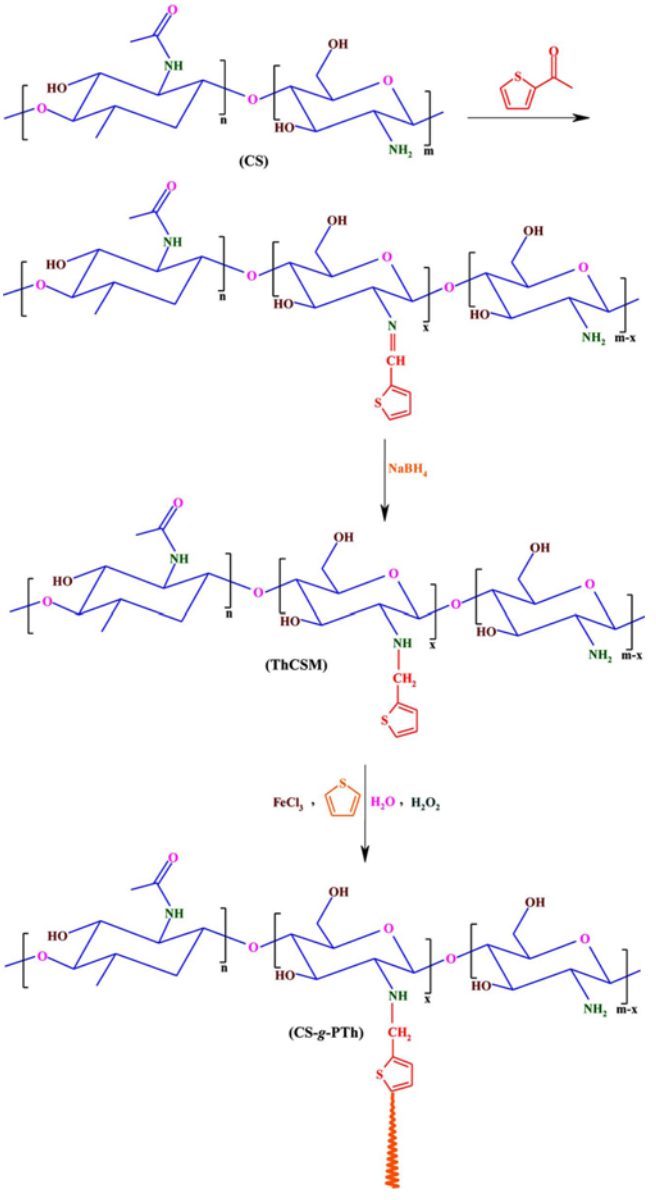

Scheme 1. Overall strategy for the synthesis of CS-*g*-PTh copolymer.

Results and Discussion

The replacement of failed tissues/organs due to injury, diseases or other type of damages is attracted more and more research efforts during the past few decades. In this context, TE is emerged as a powerful and alternative approach instead conventional methods (*e.g.*, drug therapy, mechanical devices, and surgical repair) due to its superior features as well as better clinical outcomes. As the pivotal role of scaffold in performance of a TE process, we design and fabricated two novel electrically conductive scaffolds based on CS, PTh, and PCL as shown in Schemes 1 and 2.

Characterization of Macromonomer

The chemical structure of the synthesized ThCSM macromonomer was characterized using FTIR and ^1H NMR spectroscopies as illustrated in Figures 1 and 2. The most

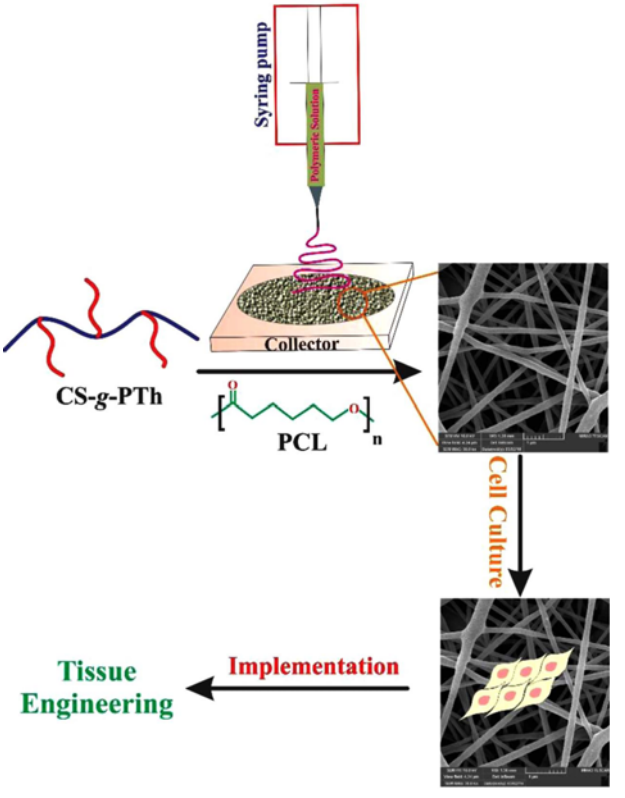

Scheme 2. Overall strategy for the fabrication of electrically conductive nanofibrous scaffolds for tissue engineering applications.

important characteristic absorption bands of CS are the stretching vibrations of the aliphatic C-H groups at 2930-2850 cm^{-1} region, the stretching vibration of amide carbonyl group at 1651 cm^{-1}, the stretching vibration of C-O group at 1073 cm^{-1}, the stretching vibration of C-N group at 1381 cm^{-1}, and the stretching vibrations of the hydroxyl and amine groups overlapped and resulted to a broad and strong band centered at 3500 cm^{-1}. The successful synthesis of thiophene-functionalized chitosan macromonomer (ThCSM) is confirmed through the appearance of some new absorption bands, including the stretching vibrations of aliphatic and aromatic C-H groups at 3020-2750 cm^{-1} region, the stretching vibrations of C=C groups at 1578 and 1502 cm^{-1}, and γ(C-H) in the aromatic ring (related to thiophene groups) at 821 and 714 cm^{-1}.

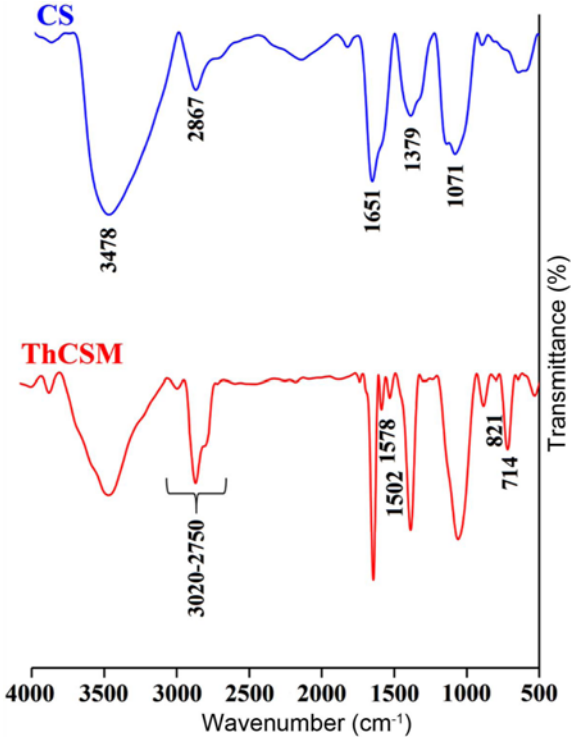

Figure 1. FTIR spectra of CS and ThCSM macromonomer.

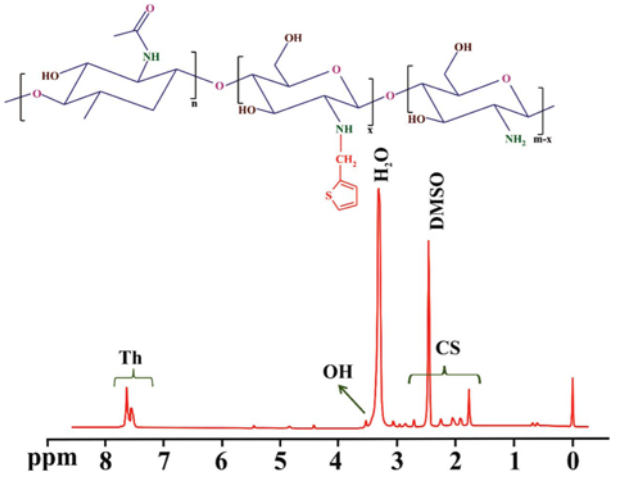

Figure 2. ^{1}H NMR spectrum of ThCSM macromonomer (DMSO-d_6 with two drop of D_2O).

Additional evidence on the successful synthesis of ThCSM macromonomer was obtained from ^{1}H NMR spectroscopy as shown in Figure 2. The small peaks appeared at 1.80-2.70 ppm are related to alkyl groups of CS, and the chemical shift at 3.65 ppm corresponded to the hydroxyl groups of CS. The chemical sifts at 7.60-7.75 ppm related to the aromatic protons of thiophene ring that confirm the successful incorporation of thiophene groups into the CS backbone. The chemical shift of NH-CH_2 group overlapped with the alkyl groups of CS.

Characterization of CS-*g*-PTh Graft Copolymer

FTIR Spectroscopy

The FTIR spectra of pure PTh and the synthesized CS-*g*-PTh graft copolymer are shown in Figure 3. The FTIR spectrum of the PTh exhibited some characteristic absorption bands, including the stretching vibrations of aromatic C-H at 3100-2950 cm^{-1} region, γ(C-H) in the aromatic ring at 1012 and 779 cm^{-1}, and the weak C-S stretching vibration at 687 cm^{-1}. The FTIR spectrum of the CS-*g*-PTh graft copolymer exhibited the combination of absorption bands of both CS and PTh. As seen, the most important bands in this spectrum are labeled.

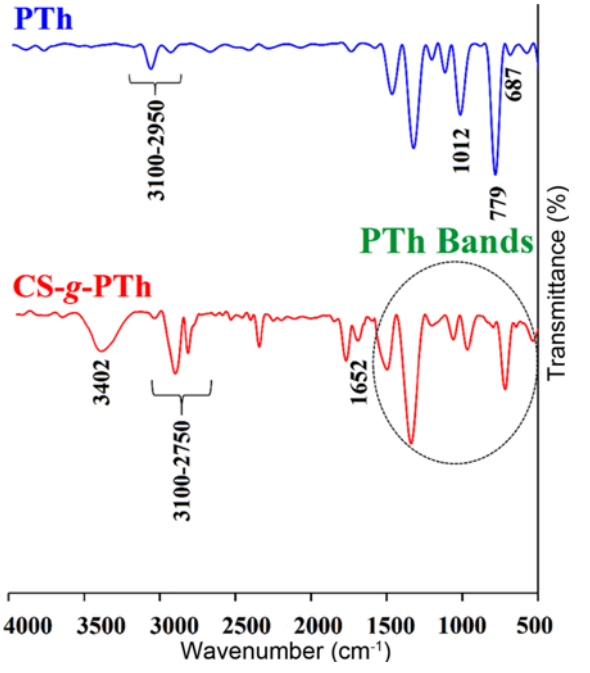

Figure 3. FTIR spectra of pure PTh and CS-*g*-PTh graft copolymer.

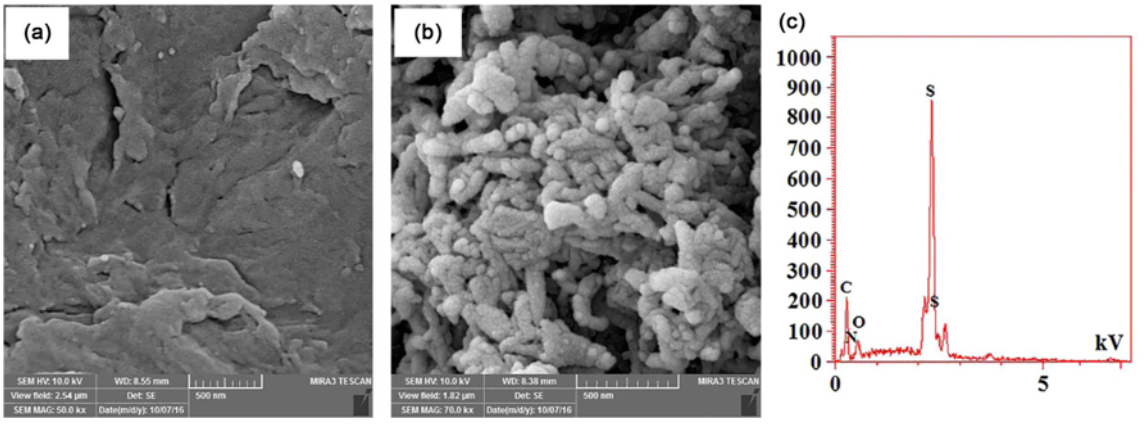

Figure 4. FE-SEM image of CS (a), and FE-SEM image (b) and EDX spectrum (c) of CS-*g*-PTh copolymer.

Table 1. Results obtained from EDX analysis of CS-*g*-PTh copolymer

Sample	C (wt.%)	N (wt.%)	O (wt.%)	S (wt.%)
CS-*g*-PTh	55.80	7.19	15.13	21.89

Surface Morphology and Chemical Composition

The surface morphologies of native CS, and the synthesized CS-*g*-PTh copolymer were observed using FE-SEM as shown in Figure 4. The FE-SEM image of native CS (Figure 4a) shows compressed plate-like morphology. In contrast, the FE-SEM image of CS-*g*-PTh copolymer (Figure 4b) exhibited the growth of PTh chains onto CS. As seen, the smooth surface of native CS was changed significantly, and some protuberances are appeared on the surface of CS. In addition, the chemical composition of the synthesized CS-*g*-PTh copolymer was investigated using energy dispersive X-ray (EDX) analysis as shown in Figure 4c, and the results obtained is summarized in Table 1.

Electrochemical Behavior

The electrochemical properties of the synthesized pure PTh and CS-*g*-PTh graft copolymer were investigated in the scan rates of 10, 20, and 30 mV s^{-1}, in the acetonitrile/TEAFB, solvent/electrolyte, couple (0.1 $molL^{-1}$), between 0.0 and +1.80 V *versus* Ag/AgCl as the reference electrode under argon protection as illustrated in Figure 5. As seen, the pure PTh exhibited a typical redox couple with anodic and cathodic peaks at approximately 1.20 and 0.70 V *versus* the reference electrode, respectively. In contrast, the anodic and cathodic peaks for the synthesized CS-*g*-PTh copolymer were observed at 1.40 and 0.80 V *versus* the reference electrode, respectively. As expected, the synthesized CS-*g*-PTh copolymer exhibited lower conductivity than those of the pure PTh due to the decreasing of conjugation length distribution with non-conductive CS.

Characterization of Electrospun Nanofibers

Morphology and Hydrophilicity

The morphology and topography of a scaffold are among

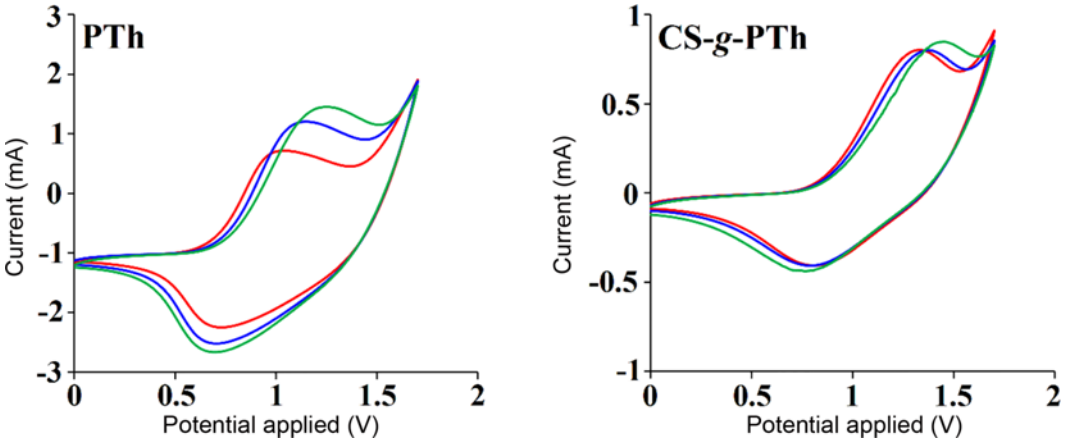

Figure 5. Cyclic voltammograms (CVs) of PTh and CS-*g*-PTh graft copolymer.

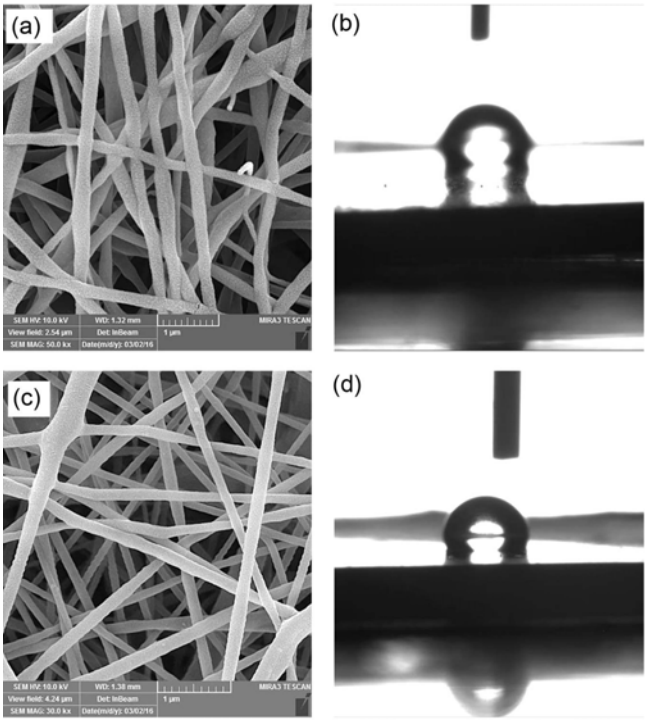

Figure 6. FE-SEM images of CS-*g*-PTh (a) and CS-*g*-PTh/PCL (c) electrospun nanofibers, as well as the photographs of water drops on CS-*g*-PTh (b) and CS-*g*-PTh/PCL (d) electrospun nanofibers.

the most important features that require for a successful TE. Therefore, the morphologies of the fabricated electrospun nanofibers were observed using FE-SEM as shown in Figure 6. As seen both nanofibers exhibited three-dimensional (3D) interconnected pore structure, with average diameters in the size range of 120±30 nm without any bead formation. Despite, the CS-*g*-PTh/PCL nanofibers shows higher uniformity than those of the CS-*g*-PTh. Therefore, the addition of a small amount of PCL lead to better morphology and topography in the fabricated nanofibers.

The surface hydrophilicity of the scaffold is another important parameter that influence its performance (*e.g.,* the extent of protein adsorption and cell attachment). The drop water contact angles of the fabricated CS-*g*-PTh (Figure 6b) and CS-*g*-PTh/PCL (Figure 6d) electrospun nanofibers were measured at ambient condition in order to investigate the surface hydrophilicites of the samples. The contact angles of the CS-*g*-PTh and CS-*g*-PTh/PCL electrospun nanofibers with water were calculated to be 83±2.8 and 89±3.1 °, respectively that exhibited acceptable hydrophilicites for TE applications. It should be pointed out that the optimal cell adhesion has been reported to polymer surfaces presenting moderate wettability with water contact angle is 40-70 ° [41], however, the promising results were also obtained for electrically conductive scaffold up to 90 ° [42,43].

Table 2. Electrical conductivities of the fabricated samples

Sample	Electrical conductivity (σ; S cm^{-1})
PTh	0.82
CS-*g*-PTh[a]	0.09
CS-*g*-PTh/PCL[a]	8×10^{-3}

[a]Electrospun nanofibers that fabricated as given in experimental section.

Electrical Conductivity Measurements

The electrical conductivity of the scaffold has pivotal role in its performance. Therefore, this property is measured before the biological tests. The electrical conductivities of the samples were investigated using the four-probe technique at ambient condition according to procedure that described in our pervious works [44,45]. As seen in Table 2, both fabricated scaffolds showed suitable electrical conductivities that qualified them for successful TE.

Biological Tests

In vitro Degradation

The degradation is one of the most important feature of scaffold. The degradation rate of scaffold should match the regeneration rate of the host tissue, and the degradation by-products must be non-toxic and readily removed from the body.

The *in vitro* degradability of the fabricated scaffolds were investigated through evaluating the morphological change using FE-SEM equipment and gravimetric measurements after soaking of nanofibers in PBS (pH 7.4) at 37 °C. The PBS was refreshed every three days. As seen in FE-SEM images (Figure 7), both fabricated CS-*g*-PTh and CS-*g*-PTh/PCL electrospun nanofibers were undergoing to swelling and degradation after 14 days incubating in PBS (pH 7.4; 37 °C). In addition, the CS-*g*-PTh/PCL sample exhibited higher degradation rate. This phenomenon is originated from the high degradation rate of PCL than PTh. In the case of gravimetric approach, at predetermined time intervals, the samples were collected, washed several times with distilled water, dried in vacuum at room temperature, and then weighted. The mass loss was calculated from: $(W_i-W_r)/W_i$ formula; where W_i and W_r are the initial and the residual dry weights of the nanofibers. The results obtained is summarized in Figure 7c. According to the results, both fabricated scaffolds showed fast mass loss in initial fourth week, and after which the degradation rate for both samples slows down. Furthermore, the CS-*g*-PTh/PCL electrospun nanofibers exhibited higher *in vitro* degradability than those of the CS-*g*-PTh electrospun nanofibers in accordance to FE-SEM images. In detail, the mass loss of CS-*g*-PTh and CS-*g*-PTh/PCL electrospun nanofibers were found to be 28.1 and 37.3 wt.%, respectively, at the end of experiments (sixth weeks).

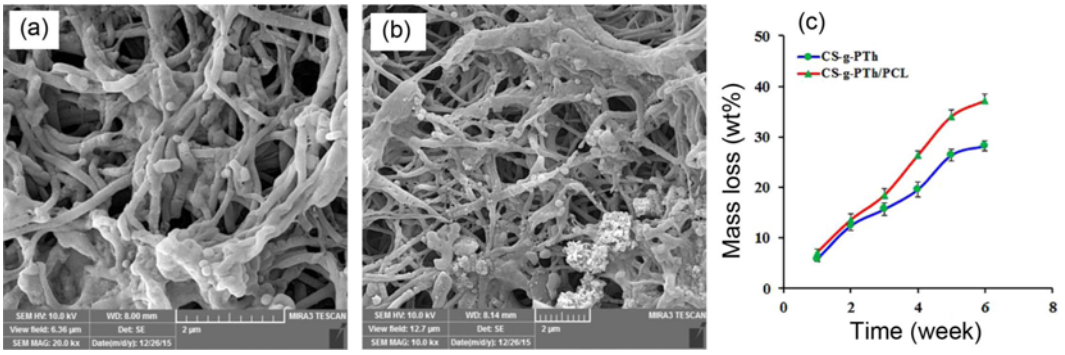

Figure 7. FE-SEM images of the CS-*g*-PTh (a) and CS-*g*-PTh/PCL (b) electrospun nanofibers after 14 days soaking in PBS (pH 7.4; 37 °C), and degradation profiles of the samples in PBS (pH 7.4; 37 °C).

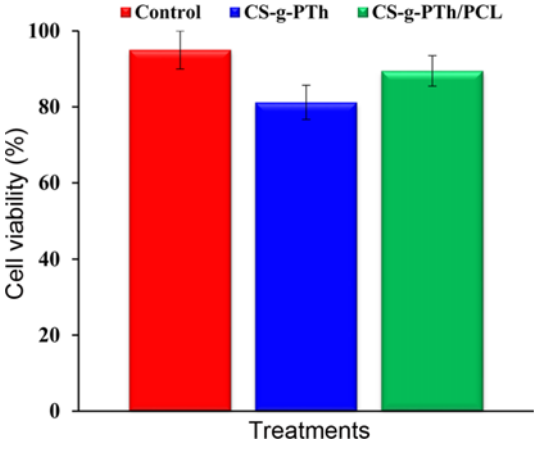

Figure 8. *In vitro* cytotoxic effects of the CS-*g*-PTh and CS-*g*-PTh/PCL electrospun nanofibers on human HEP G2 cells during 24 hours [SPSS results (P<0.05: considered statistically significant differences): Control/CS-*g*-PTh: P=0.039; Control/CS-*g*-PTh/PCL: P=0.046; and CS-*g*-PTh/CS-*g*-PTh/PCL: P=0.041].

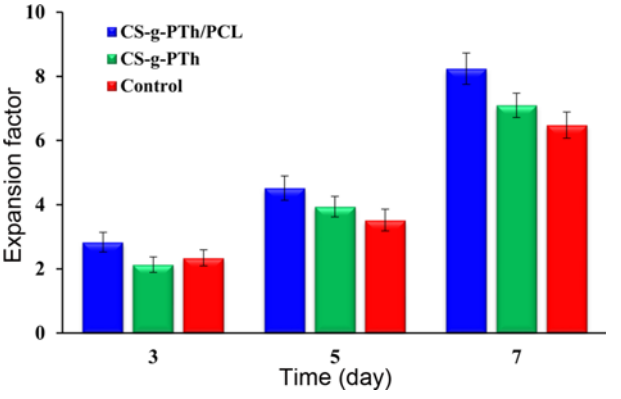

Figure 9. Performances of CS-*g*-PTh and CS-*g*-PTh/PCL electrospun nanofibers in proliferation of human HEP G2 cells [SPSS results (P<0.05: considered statistically significant differences): (3 days: Control/CS-*g*-PTh: P=0.09; Control/CS-*g*-PTh/PCL: P=0.041; CS-*g*-PTh/CS-*g*-PTh/PCL: P=0.029); (5 days: Control/CS-*g*-PTh: P=0.043; Control/CS-*g*-PTh/PCL: P=0.021; CS-*g*-PTh/CS-*g*-PTh/PCL: P=0.027); (7 days: Control/CS-*g*-PTh: P<0.020; Control/CS-*g*-PTh/PCL: P<0.001; CS-*g*-PTh/CS-*g*-PTh/PCL: P<0.001); (3/5 days ($Control_3$/$Control_5$: P<0.001; CS-*g*-PTh_3/CS-*g*-PTh_5: P<0.001; CS-*g*-PTh/PCL_3/CS-*g*-PTh/PCL_5: P<0.001); (3/7 days: ($Control_3$/$Control_7$: P<0.001; CS-*g*-PTh_3/CS-*g*-PTh_7: P<0.001; CS-*g*-PTh/PCL_3/CS-*g*-PTh/PCL_7: P<0.001); (5/7 days: ($Control_5$/$control_7$: P<0.001; CS-*g*-PTh_5/CS-*g*-PTh_7: P<0.001; CS-*g*-PTh/PCL_5/CS-*g*-PTh/PCL_7: P<0.001)].

MTT Assay

The biocompatibilities of the fabricated scaffolds as the primarily concern for biomedical applications were investigated during 24 hours using MTT assay against human HEP G2 cells. According to Figure 8, in comparison with control (polystyrene plate) both fabricated electrospun nanofibers exhibited a little bite higher toxicity, however, after mentioned incubation time the cell viability were over 80 %, indicating acceptable biocompatibilities of the fabricated scaffolds. In detail, the CS-*g*-PTh/PCL electrospun nanofibers showed higher biocompatibility in comparison with CS-*g*-PTh electrospun nanofibers. The main reason for this phenomenon may be the presence of Food and Drug Administration (FDA) approved polymer (PCL) in the sample.

Cell Growth Assay

Additional evidence on the biocompatibilities of the fabricated scaffolds as well as their performances in TE were obtained through the proliferation of human HEP G2 cells on the fabricated scaffolds. For this purpose, the cells with initial seeding density of 1×10^5 cells per cm^2 were seeded on the fabricated scaffolds, and the cells expansion were recorded during 7 days.

As seen in Figure 9, the fabricated scaffolds (especially CS-*g*-PTh/PCL) could promote cells proliferation with increasing the culture period. In detail, the CS-*g*-PTh/PCL scaffold exhibited slightly higher cells proliferation (8.24± 0.49) in comparison with CS-*g*-PTh scaffold (7.1±0.38) after 7 days. It is worth noting that in the control sample

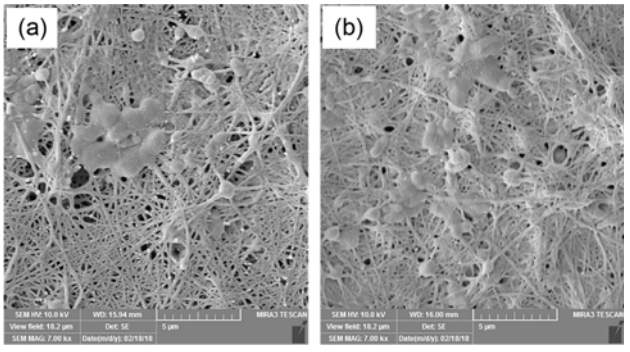

Figure 10. FE-SEM images of human HEP G2 cells on CS-*g*-PTh (a) and CS-*g*-PTh/PCL (b) electrospun nanofibers.

(polystyrene plate) the cells were expanded by a factor of 6.48±0.41 after 7 days. These results revealed the potential of the fabricated scaffolds for TE applications. The main reasons for this phenomenon can be listed as excellent attaching cites in the fabricated scaffolds due to presence of CS and PCL, excellent biocompatibility of the scaffolds, as well as intercellular communication through the electrical conductive substrate due to presence of PTh in the scaffolds.

Cell Morphology Study

The morphologies of the attached cells onto the fabricated scaffolds were observed after 24 hours incubation using FE-SEM equipment. As illustrated in Figure 10, both CS-*g*-PTh (a) and CS-*g*-PTh/PCL (b) electrospun nanofibers enhanced adhesion, spreading, and proliferation of the human HEP G2 cells. In accordance to cytotoxicity and cell growth assays, the CS-*g*-PTh/PCL scaffold exhibited higher performance in terms of adhesion, spreading, and proliferation of the cells than those of the CS-*g*-PTh scaffold as seen in FE-SEM images.

Conclusion

Two novel electrically conductive nanofibrous scaffolds namely, chitosan-*grafted*-polythiophene (CS-*g*-PTh) and chitosan-*grafted*-polythiophene/poly(ε-caprolactone) (CS-*g*-PTh/PCL), have been fabricated successfully through the electrospinning technique, and their performances in tissue engineering (TE) application were preliminary investigated in terms of some biological as well as physicochemical features. The fabricated electrospun nanofibers exhibited excellent biocompatibility and *in vitro* biodegradability as well as proper electroactivity and conductivity that qualified them as scaffolds for especial types of TE that require electroactivity. It was revealed that the addition of a small amount of PCL improves the biological features (*e.g.,* biocompatibility, biodegradability, as well as adhesion, spreading, and proliferation of the cells) of the fabricated scaffold. In contrast, the wettability of the sample was decreased through the addition of PCL. Finally, further experiments are under progress in order to evaluate the effects of electrical stimulation and electrical conductivity properties of the fabricated scaffolds on the function of the electrical stimuli-responsive cells (*e.g.,* fibroblast, neural, and osteoblast).

Acknowledgements

The authors gratefully acknowledge the financial support from Kermanshah University of Medical Sciences, Kermanshah, Iran (grant number: 980365), and Payame Noor University for technical support.

References

1. F. M. Chen and X. Liu, *Prog. Polym. Sci.,* **53**, 86 (2016).
2. B. Maher, *Nature*, **499**, 20 (2013).
3. S. Maji, T. Agarwal, J. Das, and T. K. Maiti, *Carbohyd. Polym.,* **189**, 115 (2018).
4. P. Hassanzadeh, F. Atyabi, and R. Dinarvand, *J. Control. Releas.,* **279**, 181 (2018).
5. J. Shin, E. J. Choi, J. H. Cho, A. N. Cho, Y. Jin, K. Yang, C. Song, and S. W. Cho, *Biomacromolecules*, **18**, 3060 (2017).
6. B. Kaczmarek, A. Sionkowska, J. Kozlowska, and A. M. Osyczka, *Int. J. Biol. Macromol.,* **107**, 247 (2018).
7. B. Kaczmarek, A. Sionkowska, and A. M. Osyczka, *Int. J. Biol. Macromol.,* **107**, 470 (2018).
8. H. Samadian, H. Mobasheri, S. Hasanpour, and R. Faridi-Majid, *J. Nano. Res.,* **50**, 78 (2017).
9. B. Massoumi, S. Davtalab, M. Jaymand, and A. A. Entezami, *RSC Adv.,* **5**, 36715 (2015).
10. I. Titorencu, M. G. Albu, M. Nemecza, and V. V. Jingaa, *Cur. Stem. Cell. Res. Ther.,* **12**, 165 (2017).
11. D. Ozdil and H. M. Aydin, *J. Chem. Technol. Biotechnol.,* **89**, 1793 (2014).
12. E. S. Place, J. H. George, C. K. Williams, and M. M. Stevens, *Chem. Soc. Rev.,* **38**, 1139 (2009).
13. S. G. Karaj-Abad, M. Abbasian, and M. Jaymand, *Carbohyd. Polym.,* **152**, 297 (2016).
14. J. M. Dang and K. W. Leong, *Adv. Drug. Deliv. Rev.,* **58**, 487 (2006).
15. A. Anitha, S. Sowmya, P. T. Sudheesh Kumar, S. Deepthi, K. P. Chennazhi, H. Ehrlich, M. Tsurkan, and R. Jayakumar, *Prog. Polym. Sci.,* **39**, 1644 (2014).
16. M. Swierczewska, H. S. Han, K. Kim, J. H. Park, and S. Lee, *Adv. Drug. Deliv. Rev.,* **99**, 70 (2016).
17. N. Reddy, R. Reddy, and Q. Jiang, *Tr. Biotechnol*., **33**, 362 (2015).
18. B. H. L. Oh, A. Bismarck, and M. B. Chan-Park, *Biomacromolecules*, **15**, 1777 (2014).
19. O. Garcia-Valdez, P. Champagne, and M. F. Cunningham, *Prog. Polym. Sci.,* **76**, 151 (2018).
20. D. Chow, M. L. Nunalee, D. W. Lim, A. J. Simnick, and A.

Chilkoti, *Mater. Sci. Eng R.,* **62**, 125 (2008).
21. A. A. Ghavimi, M. H. Ebrahimzadeh, M. Solati-Hashjin, and N. A. Abu-Osman, *J. Biomed. Mater. Res A.,* **103**, 2482 (2015).
22. D. Ziaud, H. Xiong, and P. Fei, *Critical. Rev. Food. Sci. Nutr.,* **57**, 2691 (2017).
23. A. M. Elbarbary, H. A. A. El-Rehim, N. M. El-Sawy, E. S. A. Hegazy, and E. S. A. Soliman, *Carbohyd. Polym.,* **176**, 19 (2017).
24. C. J. Bettinger, J. P. Bruggeman, A. Misra, J. T. Borenstein, and R. Langer, *Biomaterials,* **30**, 3050 (2009).
25. E. S. Place, N. D. Evans, and M. M. Stevens, *Nat. Mater.,* **8**, 457 (2009).
26. N. K. Guimard, N. Gomez, and C. E. Schmidt, *Prog. Polym. Sci.,* **32**, 876 (2007).
27. T. H. Qazi, R. Rai, and A. R. Boccaccini, *Biomaterials,* **35**, 9068 (2014).
28. C. Meier, I. Lifincev, and M. E. Welland, *Biomacromolecules,* **16**, 558 (2015).
29. M. R. Aufan, Y. Sumi, S. Kim, and J. Y. Lee, *ACS Appl. Mater. Interfaces.,* **7**, 23454 (2015).
30. M. S. Recco, A. C. Floriano, D. B. Tada, A. P. Lemes, R. Lang, and F. H. Cristovan, *RSC Adv.,* **6**, 25330 (2016).
31. M. Jaymand, M. Hatamzadeh, and Y. Omidi, *Prog. Polym. Sci*., **47**, 26 (2015).
32. S. Vandghanooni and M. Eskandani, *Int. J. Biol. Macromol.,* **141**, 636 (2019).
33. L. Ghasemi-Mobarakeh, M. P. Prabhakaran, and M. H. Morshed, *J. Tissue. Eng. Reg. Med.,* **5**, e17 (2011).
34. Y. Wu, L. Wang, B. Guo, Y. Shao, and P. X. Ma, *Biomaterials,* **87**, 18 (2016).
35. B. Bagheri, P. Zarrintaj, A. Samadi, R. Zarrintaj, M. R. Ganjali, M. R. Saeb, M. Mozafari, O. O. Park, and Y. C. Kim, *Int. J. Biol. Macromol.*, **147**, 160 (2020).
36. M. Hatamzadeh, P. Najafi-Moghadam, A. Baradar-Khoshfetrat, M. Jaymand, and B. Massoumi, *Polymer,* **107**, 177 (2016).
37. M. Hatamzadeh, P. Najafi-Moghadam, Y. Beygi-Khosrowshahi, B. Massoumi, and M. Jaymand, *RSC Adv.,* **6**, 105371 (2016).
38. M. Jaymand, R. Sarvari, B. Massoumi, M. Eskandani, and Y. Beygi-Khosrowshahi, *J. Biomed. Mater. Res A.,* **104**, 2673 (2016).
39. R. Sarvari, B. Massoumi, M. Jaymand, Y. Beygi-Khosrowshahi, and M. Abdollahi, *RSC Adv.,* **6**, 19437 (2016).
40. M. Eskandani, J. Abdolalizadeh, H. Hamishehkar, H. Nazemiyeh, and J. Barar, *Fitoterapia*, **101**, 1 (2015).
41. S. M. Oliveira, N. M. Alvesa, and J. F. Mano, *J. Adhes. Sci. Technol.,* **28**, 843 (2014).
42. A. Sadeghi, F. Moztarzadeh, and J. A. Mohandesi, *Int. J. Biol. Macromol.,* **121**, 625 (2019).
43. M. Li, J. Chen, M. Shi, H. Zhang, P. X. Ma, and B. Guo, *Chem. Eng. J.,* **375**, 121999 (2019).
44. M. Jaymand, *Des. Monomer. Polym.,* **14**, 433 (2011).
45. B. Massoumi, N. Sorkhi-Shams, M. Jaymand, and R. Mohammadi, *RSC Adv.,* **5**, 21197 (2015).